J. Fluid Mech. (1997), *vol.* 349, *pp.* 1–30. Printed in the United Kingdom

© 1997 Cambridge University Press

Lateral straining of turbulent boundary layers. Part 2. Streamline convergence

By N. R. PANCHAPAKESAN,[1] T. B. NICKELS,[1] P. N. JOUBERT[1] AND A. J. SMITS[2]

[1] Department of Mechanical Engineering, University of Melbourne, Parkville 3052, Australia

[2] Department of Mechanical and Aerospace Engineering, Princeton University, Princeton, New Jersey, USA

(Received 10 October 1996 and in revised form 14 March 1997)

Experimental measurements are presented showing the effects of streamline convergence on developing turbulent boundary layers. The longitudinal pressure-gradient in these experiments is nominally zero so the only extra rate-of-strain is the lateral convergence. Measurements have been made of mean flow and turbulence quantities at two different Reynolds numbers. The results show that convergence leads to a significant reduction in the skin-friction and an increase in the boundary layer thickness. There are also large changes in the Reynolds stresses with reductions occurring in the inner region and some increase in the outer flow. This is in contrast to the results of Saddoughi & Joubert (1991) for a diverging flow of the same included angle and zero pressure-gradient which show much smaller changes in the stresses and an approach to equilibrium. A new non-dimensional parameter, β_D, is proposed to characterize the local effect of the convergence and it is shown how this parameter is related to Clauser's pressure-gradient parameter, β_x. It is suggested that this is an equilibrium parameter for turbulent boundary layers with lateral straining. In the present flow case β_D increases rapidly with streamwise distance leading to a significant departure from equilibrium. Measurement of terms in the transport equations suggest that streamline convergence leads to a reduction in production and generation and large increases in mean advection. The recovery of the flow after the removal of convergence has been shown to be characterized by a significant increase in the turbulent transport of shear-stress and turbulent kinetic energy from the very near-wall region to the flow further out where the stresses have been depleted by convergence.

1. Introduction

This paper is the second part of a study on the effects of lateral straining on the development of turbulent boundary layers. The results of the first part, which considered the effects of streamline divergence, were reported by Saddoughi & Joubert (1991) (hereinafter referred to as (I)). Here, in the second part, we consider the effects of streamline convergence and attempt to draw together previous work on lateral straining in a comprehensive framework.

In the usual boundary-layer notation, the principal strain rate is $\partial U/\partial y$ and the additional lateral strain rate is $\partial W/\partial z$, which is positive for divergence and negative for convergence. Bradshaw (1973) described flows as being 'mildly' perturbed when the magnitude of the ratio $B = (\partial W/\partial z)/(\partial U/\partial y)$ is less than 0.1. When this ratio (which might be called the 'Bradshaw' parameter) exceeded 0.1, the flow was described as

being 'strongly' perturbed. As indicated in (I), very little experimental work has been performed in flows with 'simple' lateral straining, that is, lateral straining in the absence of other extra rates-of-strain (e.g. pressure gradients). For simple diverging flows, only the experiments by Sjolander (1980) on a source flow on a flat plate, and Smits, Eaton & Bradshaw (1979*a*) on a cone flow had been performed by the time (I) appeared in 1991. For simple converging flows no data were available at the time.

Since the publication of (I), preliminary results on the effect of strong convergence on a flat plate sink flow were reported by Saddoughi, Hafez & Joubert (1991) and Hafez & Joubert (1992) and a study of the effects of mild convergence and divergence in a flat plate sink/source flow was presented by Pompeo, Bettelini & Thomann (1993). All these experiments were performed on the (lateral) centreline where streamline lateral and longitudinal curvature effects were small with only very weak pressure gradients so that the effects of lateral strain could be clearly identified. The work by Saddoughi *et al.* and Hafez & Joubert was preliminary to the current study, and will be discussed in the context of the new results presented here. Pompeo *et al.* used a potential flow method to design a reversible test section with a constant free-stream velocity that was converging when the flow was in one direction and diverging when the flow was in the opposite direction. The incoming boundary layer had a Reynolds number based on momentum thickness (R_θ) of about 4800, the maximum values of B (in the middle of the layer) were about -0.22 and $+0.1$, and the skin friction coefficients changed by about -25% and $+12\%$ over the length where $\partial W/\partial z$ was non-zero. The studies by Saddoughi *et al.* and Hafez & Joubert, as well as the one presented here, were performed with initial values of R_θ at the start of convergence of about 2300 ($U_1 = 8$ m s^{-1}) and 5000 ($U_1 = 20$ m s^{-1}). The maximum values of B (in the middle of the layer) were about -0.29 and -0.24, respectively, and the skin friction coefficients decreased by about 40% for both Reynolds numbers.

The similarity parameter B, formed by the ratio of the extra strain rate to the principal strain is a local parameter, and does not provide a measure of how long the extra strain rate acts. An impulsive application of the extra strain rate e is more accurately measured by the integral of the strain rate over the time it acts (Smits, Young & Bradshaw 1979*b*), $I = \int e\,\mathrm{d}t$. For prolonged application of the extra strain rate, it is not so clear what parameter is important, especially when the level of the strain rate varies with streamwise distance, as is often the case for converging and diverging flows. In these cases, the integral definition $I_d = \int(\partial W/\partial z)\,\mathrm{d}t$ may still be useful.

Other measures can also be developed. In boundary layers with pressure gradients, Clauser defined a parameter β_x and showed that if this parameter is held constant it is possible to achieve a type of equilibrium state for boundary layers with pressure gradients acting which we shall refer to here as *approximate-equilibrium* flow. In these flows velocity-defect similarity is achieved and approximate similarity of the turbulent stresses is also possible. These flows are not true equilibrium flows, since, unless the local Reynolds number of the flow is also kept constant, it is not possible to have equilibrium for the viscous terms simultaneously. This exact equilibrium is theoretically possible in a sink-flow which may occur for a two-dimensional boundary layer in a favourable pressure gradient where the streamlines converge linearly to a point which is considered to be a two-dimensional sink.

In flows with lateral convergence or divergence it is possible to extend this approach by defining an equivalent parameter β_D which is a useful measure of the effect of convergence or divergence and is defined in terms of integral properties of the boundary layer which makes the evaluation of this parameter more accurate than

terms like $(\mathrm{d}W/\mathrm{d}z)/(\mathrm{d}U/\mathrm{d}y)$. The importance and relevance of this parameter to boundary layers with lateral convergence and divergence is discussed in this paper with particular attention paid to the possibility of equilibrium flows in which this parameter is held constant.

2. Apparatus and measurement techniques

A brief description of the experimental arrangement is given here. A more detailed description of the wind-tunnel construction may be found in (I) and in Saddoughi (1988). Details of the converging section may be found in Saddoughi *et al.* (1991) and in Hafez & Joubert (1992).

A schematic of the test section is shown in figure 1. A parallel section of rectangular cross-section was attached to the downstream end of the wind tunnel contraction. A trip wire of 0.5 mm nominal diameter was placed at the beginning of this section to cause transition and the turbulent boundary layer was allowed to develop for a distance of 1960 mm. This parallel section was followed by a section of 835 mm in length where the two sidewalls converged with a total included angle of 20°. The coordinate system was chosen so that $x = 0$ corresponds to the beginning of the converging section. A zero pressure gradient was maintained in the converging section by diverging the wall opposite the plane measurement wall to compensate for the acceleration of the flow caused by convergence. In addition to this it was found necessary to include bleeding slots at the beginning and end of the converging section to ensure zero pressure gradient over the whole of the flow. Following the converging section, a further parallel section was added with a length of 1125 mm, after which the air passed to atmosphere. In this experiment, therefore, a developed zero pressure gradient turbulent boundary layer was subjected to a simple strong lateral convergence, then allowed to recover in a further parallel section while a nominally zero pressure gradient was maintained over the whole flow. In figure 2 the variations of C_p and $\mathrm{d}C_p/\mathrm{d}x$ over the working section are plotted and it is shown that the pressure gradient is very small over the whole flow. The convergence (divergence) parameter calculated from the geometry of the flow is

$$D = \frac{1}{x - x_0}, \tag{1}$$

where x_0 is the effective origin of the converging walls and is 1730 mm for both Reynolds numbers. The divergence parameter in this flow case varies from $-0.578\ \mathrm{m}^{-1}$ to $-1.12\ \mathrm{m}^{-1}$. The variation of the spanwise strain rate divided by the mean velocity gradient at $y/\delta = 0.5$ (the 'Bradshaw parameter', B) is shown in figure 3. Since $|B| > 0.1$, the flow is considered to be strongly perturbed.

Measurements were made at two Reynolds numbers corresponding to nominal free-stream velocities of $8\ \mathrm{m\ s}^{-1}$ and $20\ \mathrm{m\ s}^{-1}$. The free-stream turbulence intensity was of the order of 0.3% for $8\ \mathrm{m\ s}^{-1}$ and 0.35% for $20\ \mathrm{m\ s}^{-1}$.

Mean flow measurements were made with a Pitot-tube of 0.73 mm diameter attached to a Gould Datametrics electronic manometer type 1014A with a Barocel pressure sensor type 572D-10W-2E3V1. Turbulence quantities were measured with cross-wire probes with platinum sensors of 5 μm diameter and 1 mm length. The sensors were arranged nominally at $\pm 45°$ and the probes were dynamically matched and calibrated using the technique developed and described by Perry (1982). The probes were connected to in-house-built hot-wire anemometers with frequency responses in excess of 25 kHz and run at an overheat ratio of two. The dynamic calibration technique also

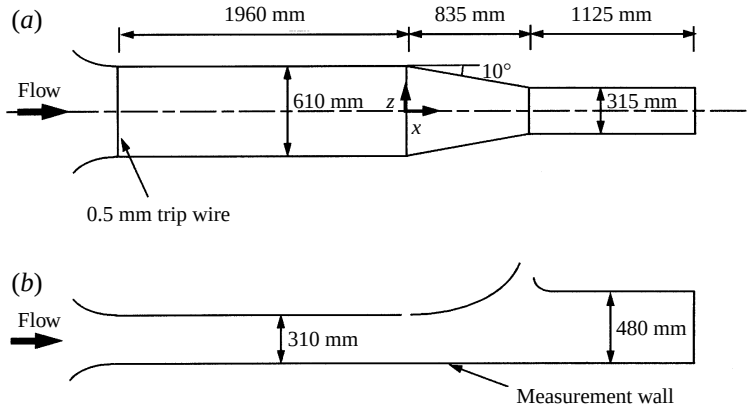

FIGURE 1. Schematic diagram of the experimental arrangement. (*a*) Elevation. (*b*) Plan.

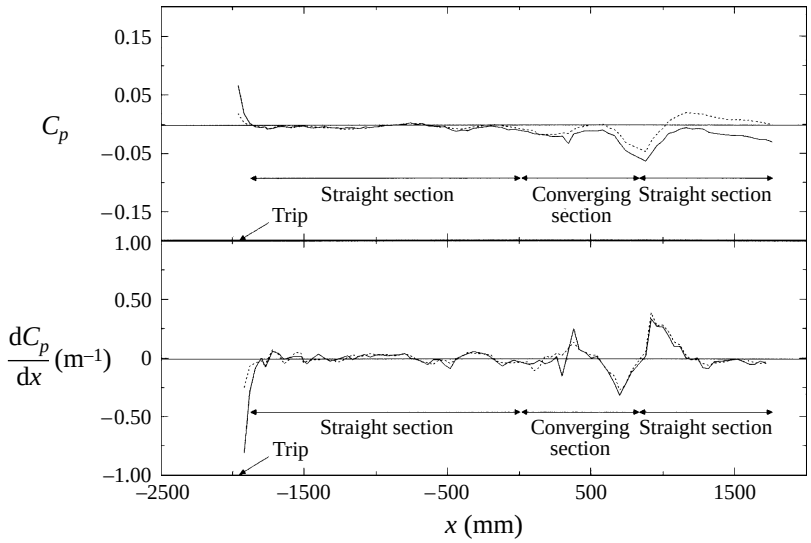

FIGURE 2. Wall-pressure distribution C_p, $\cdots$, 8 m s^{-1}, ——, 20 m s^{-1}.

provided a further test of the two-component calibration since an accurately known Reynolds stress could be imposed on the probe and compared to the measured value. Measurements were digitized using a twelve-bit data acquisition board with simultaneous sample and hold installed in a 486 PC. Checks on the calibration showed the measured values to be within $\pm 2\%$ of the actual stresses and the mean velocity to be within $\pm 0.5\%$. The streamwise skin friction measurements were made using a Preston tube of 1.05 mm diameter. The wall shear velocity used to non-dimensionalize the turbulence quantities was evaluated from the mean velocity profiles using a Clauser chart with the constants $\kappa = 0.41$ and $A = 5.2$ in the log–law formulation.

2.1. *Initial flow*

The experimental apparatus as described has an initial zero pressure-gradient section. The reason for this is that the local effect of convergence is related to the ratio of the convergence ($\mathrm{d}W/\mathrm{d}z$) to the normal-to-the-wall gradient ($\mathrm{d}U/\mathrm{d}y$). The longer the

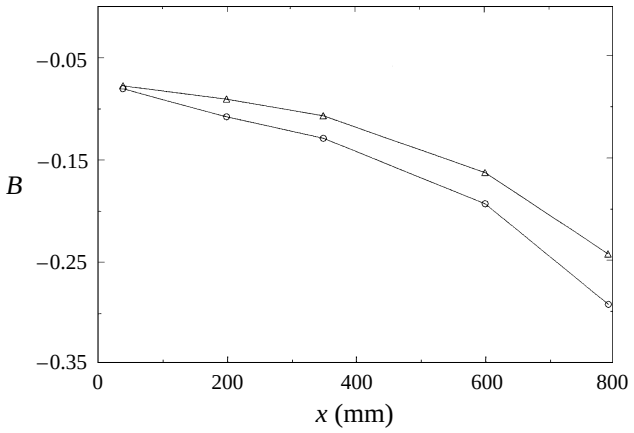

FIGURE 3. 'Bradshaw' parameter, B, evaluated at $y/\delta = 0.5$ *vs.* streamwise distance. ○, 8 m s^{-1}; △, 20 m s^{-1}.

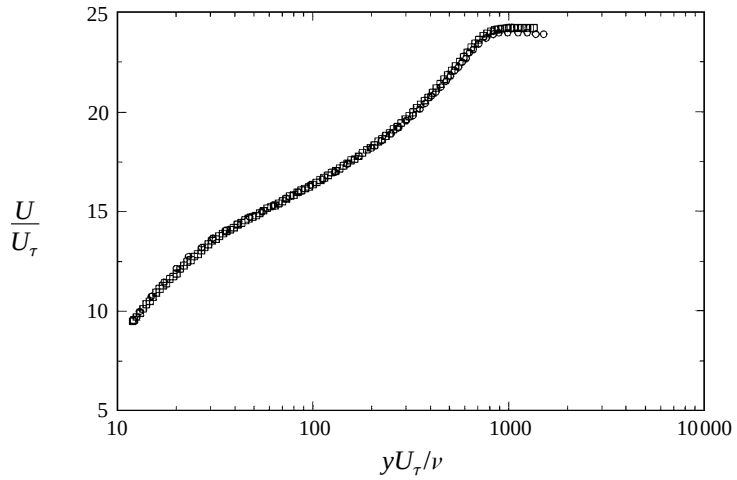

FIGURE 4. Comparison of mean velocity profile before convergence with data of Erm & Joubert (1991) at a similar R_θ. ○, Erm & Joubert $R_\theta = 2226$; □, present case $R_\theta = 2320$.

boundary layer is allowed to develop before convergence the smaller the normal-to-the-wall gradients will be. This leads to a greater effect for a fixed magnitude of convergence.

To establish that the flow before convergence was a standard two-dimensional zero pressure-gradient boundary layer, measurements were made at a station 250 mm before the start of the converging section ($x = -250$ mm). At the lower of the two velocities tested (8 m s^{-1}) the Reynolds number (based on momentum thickness) was comparable to the zero pressure-gradient measurements of Erm & Joubert (1991). The comparisons shown in figures 4 and 5 indicate a good agreement of the mean velocity profile and the Reynolds shear stress given the difference in R_θ and it appears that the boundary layer before convergence is indeed a standard two-dimensional zero pressure-gradient layer. The local skin friction coefficient (C_f') is defined by

$$C_f' = 2\tau_0/\rho U_1^2, \tag{2}$$

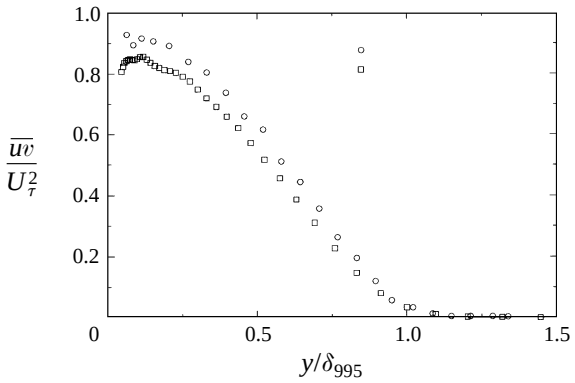

FIGURE 5. Comparison of Reynolds shear stress before convergence with data of Erm & Joubert (1991) at a similar R_θ. ○, Erm & Joubert $R_\theta = 2226$; □, present work $R_\theta = 2320$.

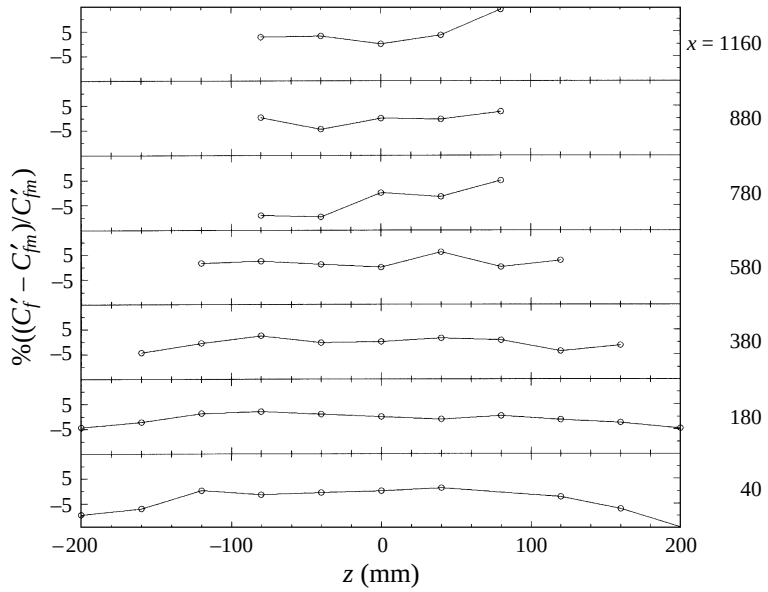

FIGURE 6. Spanwise variation of skin friction.

where τ_0 is the wall shear stress, ρ is the air density and U_1 is the free-stream velocity (i.e. the streamwise velocity outside the boundary layer). The variation of the local skin friction coefficient in the spanwise direction is shown in figure 6 for the 20 m s^{-1} case. On this figure C_{fm}' is the value of C_f' on the tunnel centreline. Measurements are shown only for this case since the results should be more accurate than the 8 m s^{-1} case owing to the larger dynamic head. The results should be independent of Reynolds number since they essentially depend only on the geometry of the apparatus. The variation near the centreline is small suggesting that the mean flow is nominally two dimensional.

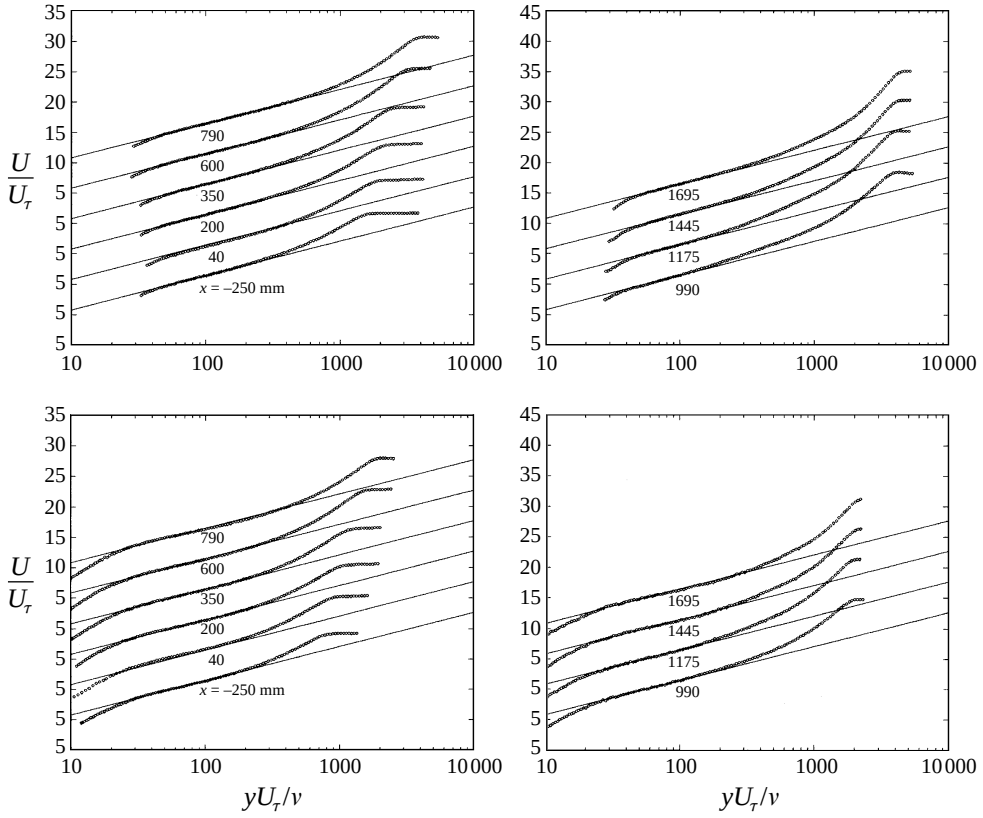

FIGURE 7. Centreline mean velocity plots, top 20 m s^{-1}, bottom 8 m s^{-1}. Plots on left-hand side show inlet and converging flow. Plots on right-hand side show recovery region.

3. Mean flow measurements

The mean velocity profiles are shown in figure 7. All the profiles show logarithmic regions with a wake component that increases in the converging section. Also shown on these plots is the logarithmic profile given by

$$\frac{U}{U_\tau} = \frac{1}{0.41}\ln\frac{yU_\tau}{\nu} + 5.2, \tag{3}$$

where $U_\tau = (\tau_0/\rho)^{1/2}$. It appears from these plots that, apart from the increase in the wake, the shape of these profiles is not very different from boundary-layer profiles in the absence of convergence.

3.1. *Streamwise development*

Figure 8 shows the variation of Coles wake parameter with streamwise distance. The variation seems to be approximately independent of Reynolds number except for a vertical shift. The rate-of-change of Π is virtually unchanged in the converging section, although some difference between the two cases occurs in the recovery section.

The variation of C_f' with streamwise distance for both cases is shown in figure 9. Also shown are calculations for a two-dimensional zero pressure-gradient layer (i.e. a boundary without streamline convergence) using the method of von Kármán (1932). The skin friction in the region of convergence drops much more rapidly with streamwise

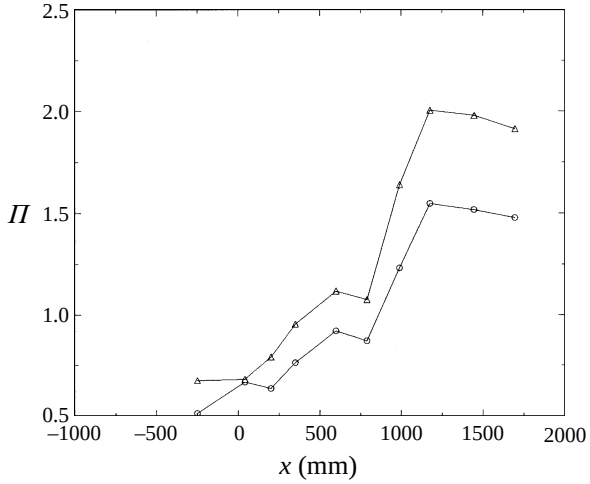

FIGURE 8. Variation of Coles wake parameter, Π, with x_s ○, 8 m s^{-1}; △, 20 m s^{-1}.

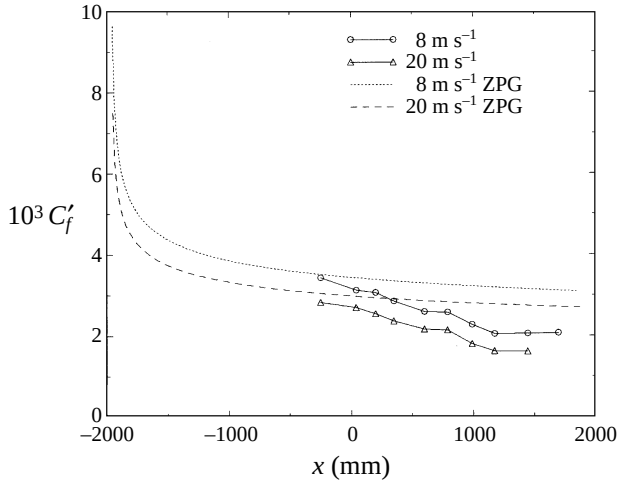

FIGURE 9. Skin friction coefficient, $C_f' = \tau_0/(0.5\rho U_1^2)$ *vs.* streamwise distance, x. Prediction for two-dimensional zero-pressure gradient layer. · · ·, 8 m s^{-1}; – – –, 20 m s^{-1}.

distance than the flow without convergence but seems to 'flatten out' in the recovery section ($x > 790$ mm). An interesting point is that the shape of the two experimental curves is nearly identical apart from a vertical shift. It appears that the rate-of-change of the skin-friction with streamwise distance in the converging section does not appear to change significantly with the change in Reynolds number in this experiment.

The variation of the integral parameters of the boundary layer is shown in figure 10. Also shown on these plots is the variation for a zero pressure-gradient boundary layer as measured by Erm & Joubert (1991) for a free-stream velocity of 8 m s^{-1} and the same virtual origin. These results are directly comparable with those for the lower of the two Reynolds numbers examined here. The values for all the integral parameters are very close to those of Erm & Joubert (1991) before the start of the converging section, as would be expected. The plots show a rapid increase of the boundary-layer thickness (in both θ and δ) that leads to an increase in R_θ. Of particular interest is the shape factor which appears to be approximately constant over the region of convergence and

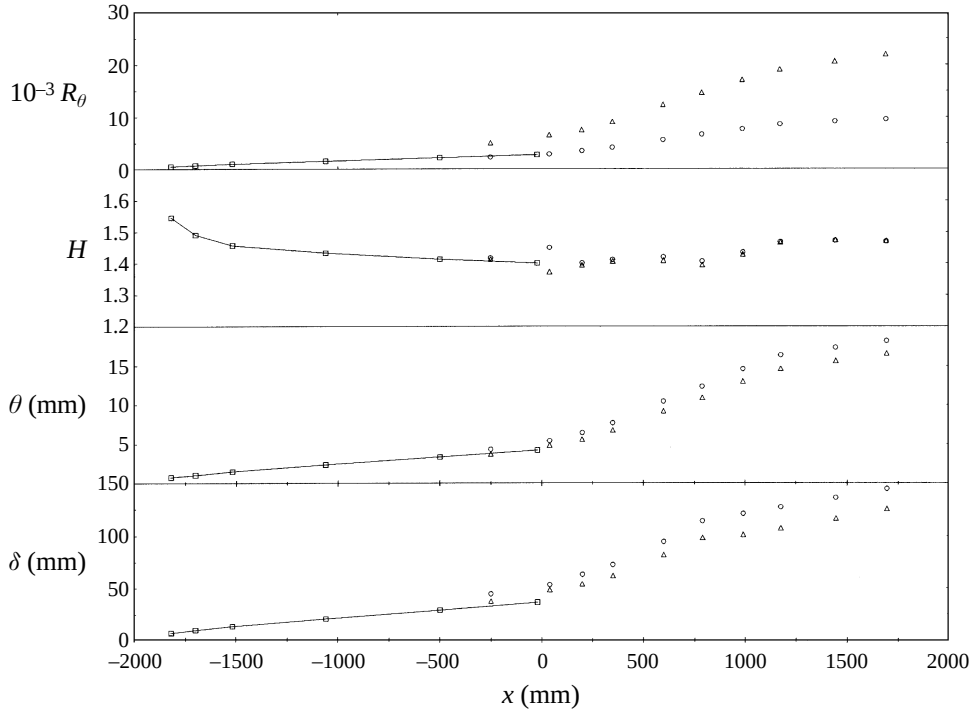

FIGURE 10. Integral parameters: □, measurements of Erm & Joubert ZPG 8 m s^{-1}; ○, present case 8 m s^{-1}; △, present case 20 m s^{-1}.

independent of Reynolds number, even though the mean velocity profiles are changing shape. This is also seen in the results of Saddoughi & Joubert (1991) for the case of divergence. It seems then that the effect of convergence or divergence on the shape parameter is not large in comparison to that observed in flows with pressure gradients. A nearly constant shape factor was also observed by Pompeo *et al.* (1993), although they state that the shape factor was increased slightly by convergence and decreased slightly by divergence. Their plots show a 3.5% increase for the converging flow and a 1.5% decrease for the diverging flow.

4. A parameter to characterize convergence and divergence

The behaviour of the mean velocity profiles and the wake parameter is similar to that observed in adverse pressure-gradient flows. In fact, in the absence of other information, it would be difficult to tell from these mean velocity plots whether this was an adverse pressure-gradient flow or a converging flow. This is not surprising since a consideration of the continuity equation for both flows shows that both extra strains applied separately are equivalent to $\mathrm{d}V_1/\mathrm{d}y$, i.e. the gradient of the mean normal to the wall velocity component in the free stream.

$$\frac{\mathrm{d}U_1}{\mathrm{d}x} = -\frac{\mathrm{d}V_1}{\mathrm{d}y} \tag{4}$$

for a two-dimensional adverse or favourable pressure-gradient flow and

$$\frac{\mathrm{d}W_1}{\mathrm{d}z} = -\frac{\mathrm{d}V_1}{\mathrm{d}y} \tag{5}$$

for a converging or diverging zero pressure-gradient flow (the subscript '1' refers to conditions outside the boundary layer).

A significant advance in the understanding of boundary layers with pressure gradients was made by Clauser (1954) who pointed out that an appropriate parameter to characterize the pressure gradient could be defined by considering the forces on a fluid element. He defined a parameter β_x as

$$\beta_x = \frac{\delta^*}{\tau_0}\frac{\mathrm{d}P}{\mathrm{d}x} = -\frac{\delta^*}{U_\tau}S\frac{\mathrm{d}U_1}{\mathrm{d}x} = \frac{\delta^*}{U_\tau}S\frac{\mathrm{d}V_1}{\mathrm{d}y}, \tag{6}$$

where $S = U_1/U_\tau$ and (4) has been used. Although Clauser (1954) originally derived this parameter by considering the ratio of skin-friction force to pressure-gradient force it can also be considered to be a ratio of the extra rate-of-strain due to the pressure-gradient to the primary rate-of-strain of the boundary layer.

It is possible to extend this idea to flows with lateral streamline convergence or divergence by noting the equivalence given by (5) and defining an equilibrium parameter β_D by

$$\beta_D = -\delta^* S^2 \frac{1}{U_1}\frac{\mathrm{d}W_1}{\mathrm{d}z} = -\delta^* S^2 D, \tag{7}$$

where D is the 'divergence' parameter defined earlier and for simple divergence (i.e. not varying through the layer) which is the present case then $D = (1/U_1)\,\mathrm{d}W_1/\mathrm{d}z$. Thus β_D is effectively a measure of the divergence of the streamlines in the outer flow in a centreline plane.

Physically, β_D can be interpreted as either a ratio of the extra rate-of-strain due to streamline convergence (or divergence) to the principal rate-of-strain, $\partial U/\partial y$, or as a ratio of the timescale of the large eddies in the flow (δ/U_τ) to the timescale of the extra rate-of-strain ($1/(\mathrm{d}W/\mathrm{d}z)$). If an extra rate-of-strain is added to (or removed from) an existing boundary layer then this ratio gives an indication of the time it will take for the boundary layer to adjust to the new condition. One advantage of this definition over the Bradshaw parameter, B, defined earlier is that it is defined in terms of integral properties of the boundary layer which may be measured more accurately than local gradients.

The variation of β_D is shown in figure 11. It may be noted that the difference between the two Reynolds numbers is small. Also shown on this figure are the values of β_D calculated for the converging flow of Pompeo *et al.* (1993) and for the diverging flow of Saddoughi & Joubert (1991). The magnitude of β_D in the present experiment is much larger than in the other experiments and the rate of change of β_D with x is also large. A further point to note from the figure is that, in the diverging flow, the change in β_D is small over the whole flow and at large x it becomes approximately constant. It is reasonable to suggest that if β_D is kept constant in this flow it may be possible to achieve an equilibrium layer in the same way that pressure-gradient flows with constant β_x can achieve equilibrium (or at least a close-to-equilibrium state). The results of Saddoughi & Joubert (1991) show very little change in the non-dimensional stresses, particularly at large x and also the value of Cole's wake factor, Π, becomes constant suggesting that this flow (with approximately constant β_D) is close to equilibrium. The authors state that beyond $x \approx 35\delta_0$ (where δ_0 is the initial boundary-layer thickness) that 'apparently…the boundary layer had reached a state of equilibrium'. The conditions required for equilibrium can be derived and used to show that an *approximate-equilibrium* boundary layer is possible for turbulent boundary layers with

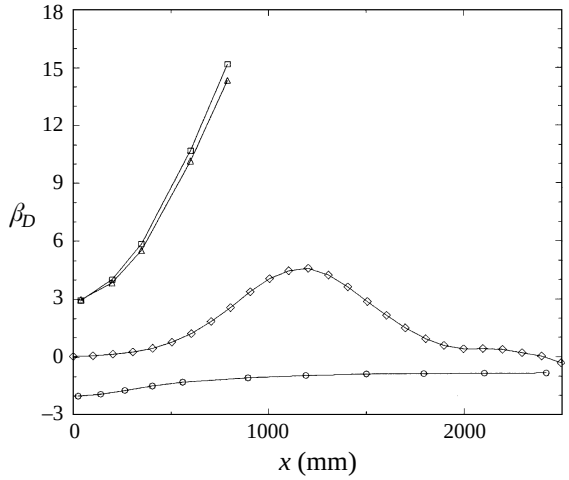

FIGURE 11. β_D *vs.* streamwise distance. ○, Saddoughi layer C 8 m s^{-1}; △, converging 8 m s^{-1} current experiment; □, converging 20 m s^{-1} current experiment; ◇, Pompeo *et al.* converging 42 m s^{-1}.

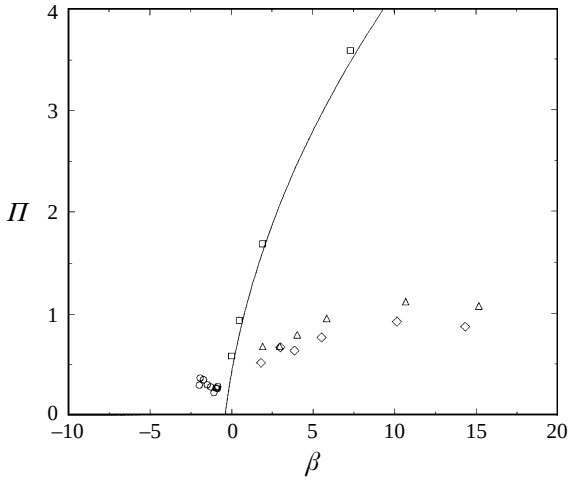

FIGURE 12. Coles wake factor Π versus β. ○, diverging flow of Saddoughi; □, East's equilibrium data; △, present case 20 m s^{-1}; ◇, present case 8 m s^{-1}; ——, curve fit of Das (1987).

simple linear divergence if the parameter β_D is held constant. It can be further shown that exact equilibrium is possible if $\beta_D/H = -1$ where H is the shape factor (for a detailed discussion of these conditions see Nickels & Joubert 1997). In the present case with simple linear convergence and zero pressure-gradient, it can also be shown that equilibrium (either approximate or exact) is not possible since it is not possible to keep β_D constant. Since the definition of β_x in two-dimensional boundary layers with pressure gradients is equivalent to β_D in a flow with zero pressure gradient the relationship of Π versus β (where β represents β_x or β_D where appropriate) is shown in figure 12 compared with the adverse pressure-gradient results of East, Sawyer & Nash (1979) for equilibrium layers. Also shown on this figure is the curve-fit of Das (1987) which has been found by curve-fitting a large amount of data. The results for

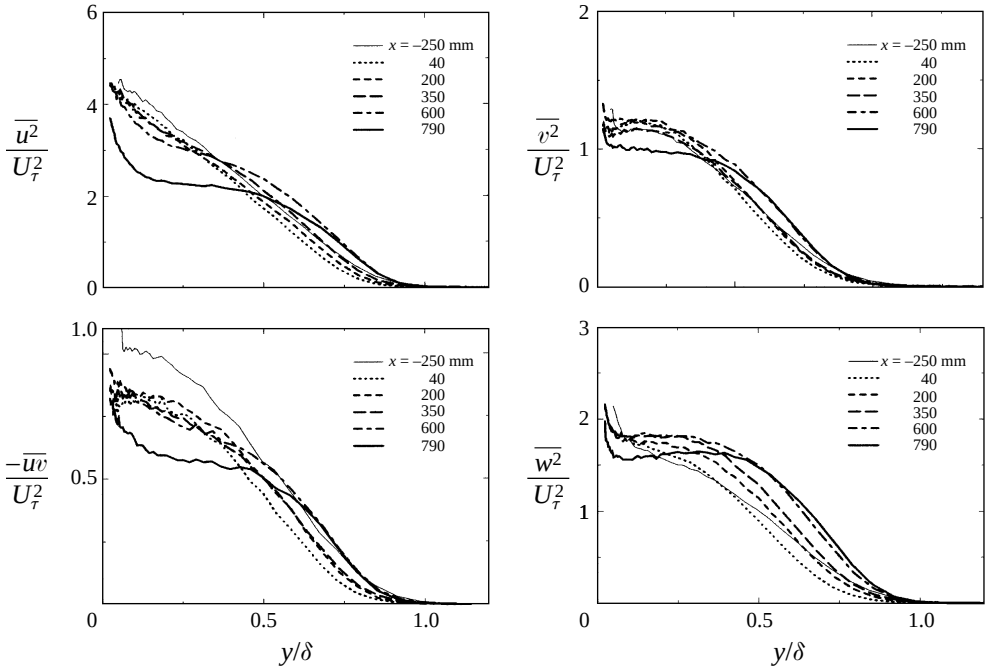

FIGURE 13. Reynolds stresses 20 m s^{-1} case in converging region.

the diverging flow of Saddoughi & Joubert (1991) are close to this curve and seem to approach it more closely at large streamwise distances (as β_D becomes constant). The results for the converging flow are far from this curve with the difference increasing with streamwise distance which may well be due to the fact that the flow is far from equilibrium since $\mathrm{d}\beta/\mathrm{d}x$ is large.

5. Reynolds stresses

In this section the turbulence quantities presented are for the 20 m s^{-1} flow case. The behaviour of all the quantities is very nearly the same for the 8 m s^{-1} and 20 m s^{-1} flow cases. The data for the 8 m s^{-1} flow case is available from the authors.

The behaviour of the turbulence intensities, shear stresses and the turbulent kinetic energy is shown in figures 13–15. Some main points may be noted. In the converging section all components show a reduction in the inner region corresponding approximately to $0.1 < y/\delta < 0.4$. There also appears to be an overall increase in the normal components in the outer region, although the trend is not monotonic with some reduction in the outer region occurring initially. While the streamwise component ($\overline{u^2}$) and the Reynolds shear stress show the maximum overall reduction, it is the profile of the spanwise component ($\overline{w^2}$) that shows the most significant change in shape corresponding to a large increase in the outer region, coupled with a reduction in the inner part. All components develop an approximately 'flat' region in the inner flow by the end of the convergence.

In the recovery region the trends are less obvious, but all components seem to exhibit a reduction in the length of the 'flat' region with streamwise distance. This appears to be dominated by a relative increase in the quantities toward the wall although there is also some decrease in the outer flow.

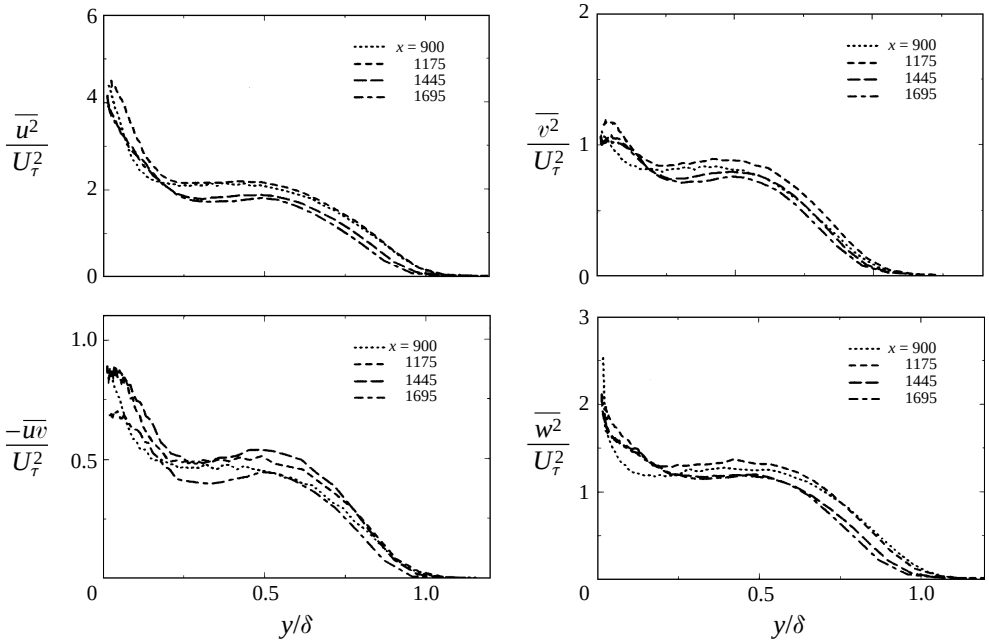

FIGURE 14. Reynolds stresses 20 m s^{-1} case in recovery region.

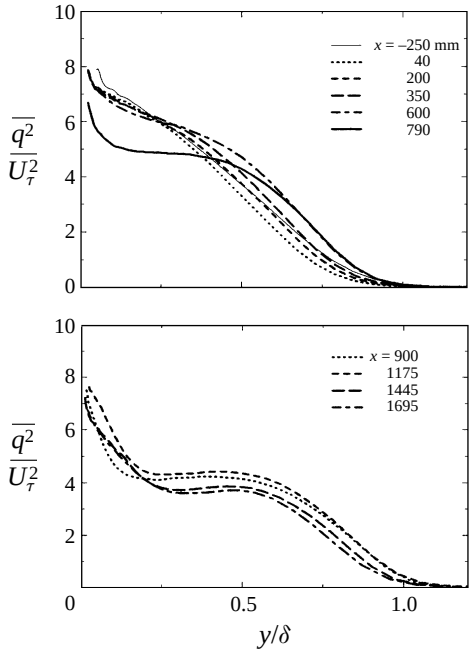

FIGURE 15. Turbulent kinetic energy. Top converging section, bottom recovery section, 20 m s^{-1}.

The trends in the turbulent kinetic energy reflect the changes in the individual components and hence exhibit the same overall trends.

6. Transport of kinetic energy and shear-stress

In order to gain some insight into the behaviour of the flow subjected to convergence the transport equations for shear stress and turbulent kinetic energy may be examined. They may be written in the following forms,

$$\tfrac{1}{2}\delta(S-f)\frac{\partial(-\overline{uv}/U_\tau^2)}{\partial x} =$$
$$(S-f)\frac{\delta}{S}\frac{\mathrm{d}S}{\mathrm{d}x}\frac{-\overline{uv}}{U_\tau^2}-\frac{1}{2}\left(\frac{\mathrm{d}\delta}{\mathrm{d}x}(I_1-\eta f)-\frac{\delta}{S}\frac{\mathrm{d}S}{\mathrm{d}x}I_1+\frac{\beta_D}{C_1}\eta\right)\frac{\partial-\overline{uv}/U_\tau^2}{\partial\eta}\Bigg]A$$
$$-\frac{-\overline{uv}}{U_\tau^2}\frac{\beta_D}{C_1}-\frac{\overline{v^2}}{U_\tau^2}f'\Bigg]B$$
$$-\eta\frac{\partial\overline{u^2v}/U_\tau^3}{\partial\eta}\frac{\partial\delta}{\mathrm{d}x}-3\frac{\overline{u^2v}}{U_\tau^3}\frac{\delta}{S}\frac{\mathrm{d}S}{\mathrm{d}x}+\frac{\partial}{\partial\eta}\left(\frac{\overline{uv^2}}{U_\tau^3}\right)\Bigg]C$$
$$-\frac{\delta}{U_\tau^3}\left(\overline{\frac{p'}{\rho}\left(\frac{\partial u}{\partial y}+\frac{\partial v}{\partial x}\right)}\right)\Bigg]D \tag{8}$$

for the Reynolds shear stress, and

$$\tfrac{1}{2}\delta(S-f)\frac{\partial(\overline{q^2}/U_\tau^2)}{\partial x} =$$
$$(S-f)\frac{\delta}{S}\frac{\mathrm{d}S}{\mathrm{d}x}\frac{\overline{q^2}}{U_\tau^2}-\frac{1}{2}\left(\frac{\mathrm{d}\delta}{\mathrm{d}x}(I_1-\eta f)-\frac{\delta}{S}\frac{\mathrm{d}S}{\mathrm{d}x}I_1+\frac{\beta_D}{C_1}\eta\right)\frac{\partial\overline{q^2}/U_\tau^2}{\partial\eta}\Bigg]E$$
$$-\frac{-\overline{uv}}{U_\tau^2}f'-\left(\frac{\overline{u^2}}{U_\tau^2}-\frac{\overline{v^2}}{U_\tau^2}\right)\left(\frac{\mathrm{d}\delta}{\mathrm{d}x}\eta f'+\frac{\delta}{S}\frac{\mathrm{d}S}{\mathrm{d}x}f\right)+\left(\frac{\overline{w^2}}{U_\tau^2}-\frac{\overline{v^2}}{U_\tau^2}\right)\frac{\beta_D}{C_1}\Bigg]F$$
$$+\frac{1}{2}\left(\eta\frac{\partial}{\partial\eta}\left(\frac{\overline{\alpha^3}}{U_\tau^3}\right)+3\frac{\overline{\alpha^3}}{U_\tau^3}\frac{\delta}{S}\frac{\mathrm{d}S}{\mathrm{d}x}\right)-\frac{3}{4}\frac{\partial}{\partial\eta}\left(\frac{\overline{u^2v}}{U_\tau^3}+\frac{\overline{v^3}}{U_\tau^3}\right)\Bigg]G$$
$$-\frac{\epsilon\delta}{U_\tau^3}\Bigg]H \tag{9}$$

for the turbulent kinetic energy, where $\eta = y/\delta$ and

$$\overline{\alpha^3} = \overline{u^3}+\overline{uv^2}+\overline{uw^2}, \tag{10}$$

$$f = \frac{U_1-U}{U_\tau} \tag{11}$$

is the defect profile and

$$I_1 = \int_0^\eta f\,\mathrm{d}\eta. \tag{12}$$

The labelled terms in (8) are *A*, transport by mean-flow; *B*, generation; *C*, transport by velocity fluctuations; *D*, redistribution by pressure fluctuations. In (9) they are *E*, advection by the mean flow; *F*, production; *G*, diffusion by velocity fluctuations; *H*, dissipation.

In the Reynolds shear-stress equation the transport and redistribution due to viscous

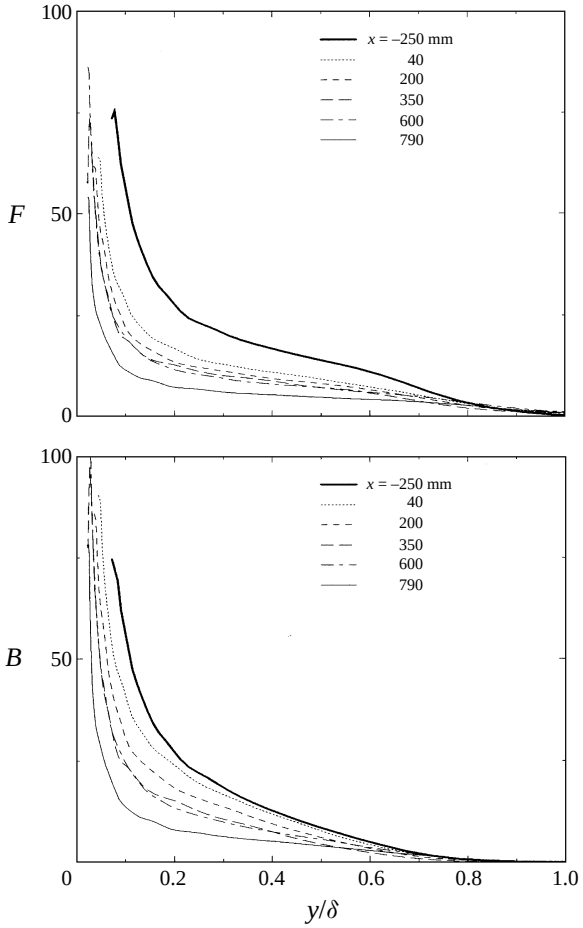

FIGURE 16. Production of turbulent kinetic energy and generation of shear stress in converging region.

forces have been neglected, as has the transport by pressure fluctuations, although the redistribution due to pressure fluctuations has been retained. In the energy equation, the pressure diffusion term has been neglected and it was assumed that $\overline{uw^2} = \frac{1}{2}(\overline{u^2v} + \overline{v^3})$. These approximations have been discussed by Bradshaw (1967) and Lawn (1971). In the form presented here, these equations show directly the effect of the various terms on the rate of change of the quantities ($\overline{q^2}$ and $-\overline{uv}$) with respect to streamwise distance.

Inspection of the first equation suggests that convergence leads to a reduction in the generation of shear stress and an increase in the advection of the shear stress away from the wall since β_D occurs explicitly in these two terms. In the second equation, the advection is also increased and it would appear that the production is also increased by the extra term containing β_D. It should be noted, however, that the production also depends directly on the value of the Reynolds shear stress and hence depends on the changes in shear stress which result from the transport in the first equation. Similarly, the rate of generation of Reynolds shear stress depends on $\overline{v^2}$ which is related to the magnitude of the turbulent kinetic energy. In the following sections the effects of convergence on the terms in equations (8) and (9) are discussed. The abscissa of each plot is labelled with the letter that corresponds to the appropriate term in the above

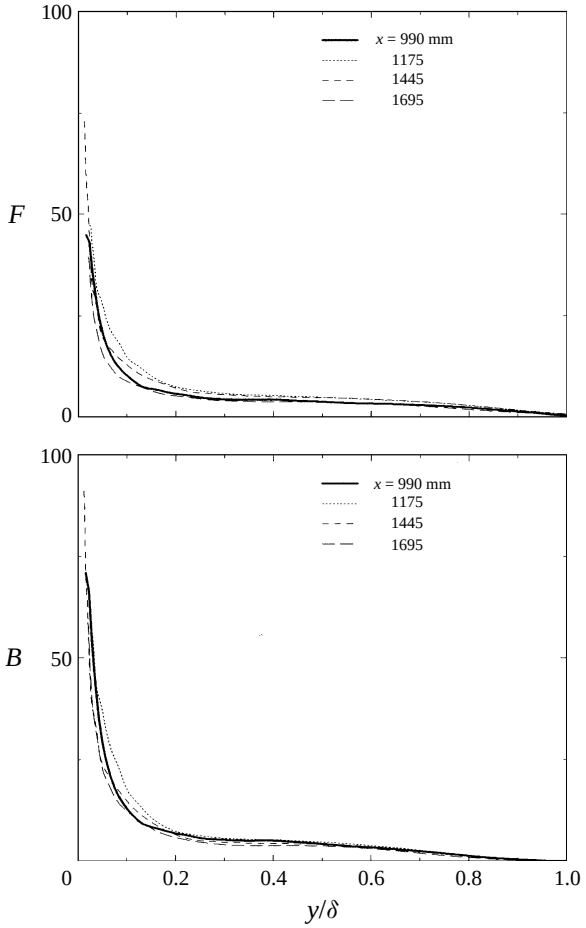

FIGURE 17. Production of turbulent kinetic energy and generation of shear stress in recovery region.

equations. Each term has been divided by $\delta(S-f)$ so they can be considered to be the contributions of the various processes to $\partial(\overline{q^2}/U_\tau^2)/\partial x$ and $\partial(\overline{-uv}/U_\tau^2)/\partial x$. All terms except D and H have been measured directly.

6.1. *Production and generation*

As has been stated above, the convergence parameter, β_D, explicitly affects the production and generation terms, as well as increasing the mean advection of these quantities. The changes in these terms are the direct effects of convergence on the turbulence quantities. Figure 16 shows the changes in the production and generation terms in the converging section. Overall, the effect of convergence is to reduce the magnitude of both these terms. In the recovery section shown in figure 17 the changes are much smaller. There is no obvious recovery in the production suggesting that if this is occurring it is a slow process. In order for the production (and generation) to increase to the value before convergence it is necessary for the stresses to recover and this recovery depends on the timescale of the large eddies in the boundary layer.

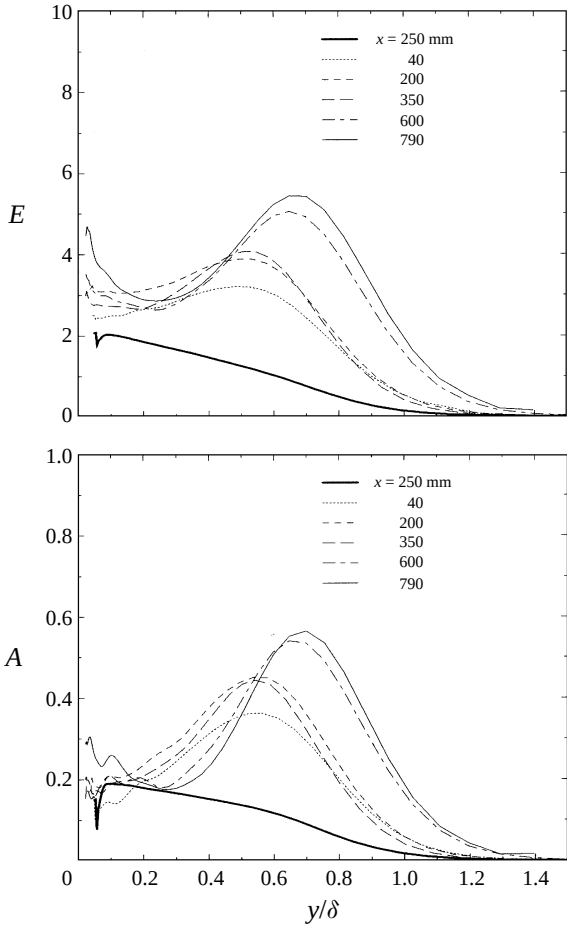

FIGURE 18. Advection of turbulent kinetic energy and shear stress in converging region.

6.2. *Advection by the mean flow*

The changes in the advection of both shear stress and turbulent kinetic energy due to convergence are quite marked as shown in figure 18. Both show a large increase in the outer region of the flow as soon as convergence is applied. The peak gain due to advection moves away from the wall with streamwise distance. The reason for this behaviour may be understood from the transport equations. The explicit term containing β_D in both equations depends on the normal-to-the-wall gradient multiplied by the non-dimensional distance from the wall ($\eta\partial/\partial\eta$). This leads to an increase in the outer part of the flow which reduces the gradients in the inner region. Hence the position of the maximum gradient moves away from the wall. This process aids in the formation of the 'flat' region in the stresses discussed above.

In the recovery section the advection is substantially reduced and appears to become slightly negative, as shown in figure 19. The negative value probably arises because of the inaccuracy in the measurement of the streamwise gradients and may not be significant. The overall reduction is, however, a real, and direct, consequence of the removal of the extra rate of strain.

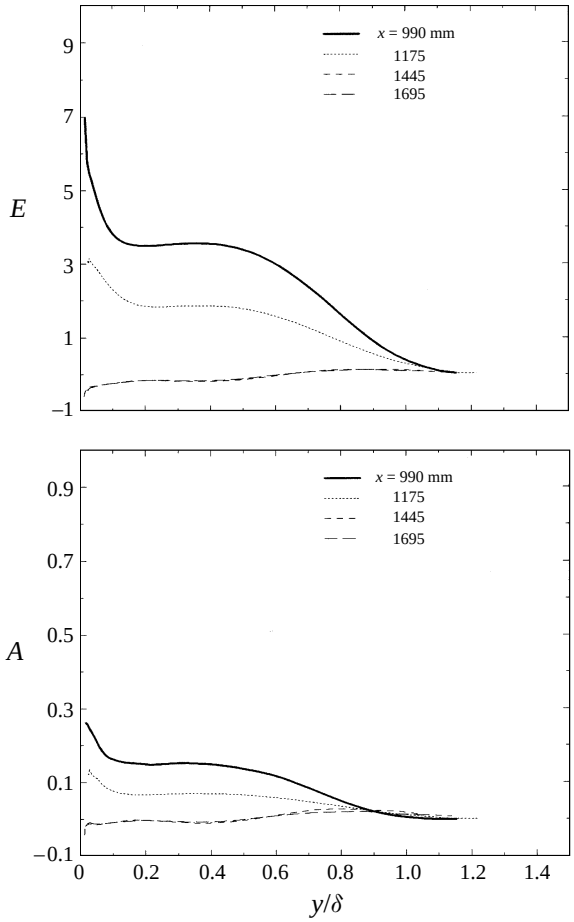

FIGURE 19. Advection of turbulent kinetic energy and shear stress in recovery region.

6.3. *Turbulent transport and diffusion*

The turbulent transport and diffusions terms correspond to the transport of the appropriate quantity by the velocity fluctuations. The results are shown in figures 20 and 21. The turbulent transport or diffusion may be considered to be a response of the boundary layer to the changes caused by convergence. In the converging region there is a gradual increase in this transport in the inner region and a reduction in the outer region. These trends are opposite to those observed for the advection. It is worth noting that the increase in the inner region does not occur immediately the convergence is applied (in fact there appears to be a small reduction in the transport of kinetic energy at the first station). The changes are much less dramatic than the changes in advection. It appears then that the boundary layer responds to the increased advection and reduced production by reducing the gain due to turbulent transport or diffusion in the outer region and reducing the loss due to turbulent transport in the inner region. The timescale of this response depends on the timescale of the large eddies and hence there is a time-lag between the external changes and the changes in turbulent transport.

In the recovery region there is a distinct change in the behaviour of the transport near the wall. The transport terms for both shear stress and turbulent kinetic energy

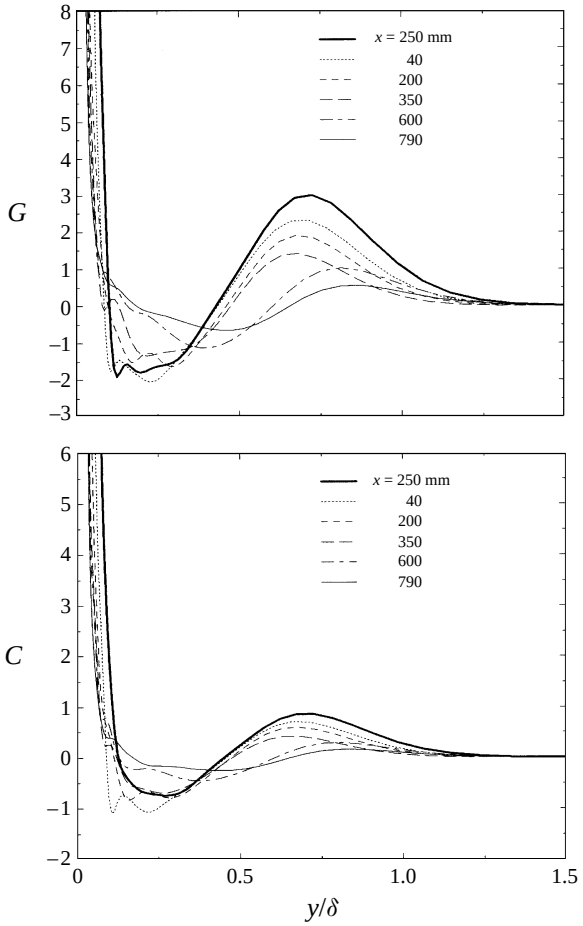

FIGURE 20. Diffusion of turbulent kinetic energy and turbulent transport of shear stress in converging region.

show a rapid reduction near the wall leading to a sharp negative peak (loss) around $\eta = 0.05$ followed by a positive peak (gain) further out at around $\eta = 0.13$. This indicates a significant transfer from the very near-wall region to the region further out where the stresses have been depleted. This is a definite indication of the recovery process and explains the observation that the beginning of the 'flat' region in the stresses moves out from the wall during recovery. The transport in the outer flow also shows a negative region around $0.5 < \eta < 0.6$ followed by a positive region further out. This difference indicates transfer away from the wall and this transport is seen to reduce with streamwise distance in the recovery region.

6.4. *Dissipation and redistribution*

These two terms may be considered to be the 'sink' terms in the transport equations in that both terms are negative across the layer and hence tend to reduce the transported quantities. The dissipation of the turbulent kinetic energy could not be measured in the present experiment although it can be found by difference using the transport equations. The accuracy of this procedure depends on the importance of the terms that have been neglected in the equations and so the results are not plotted. It

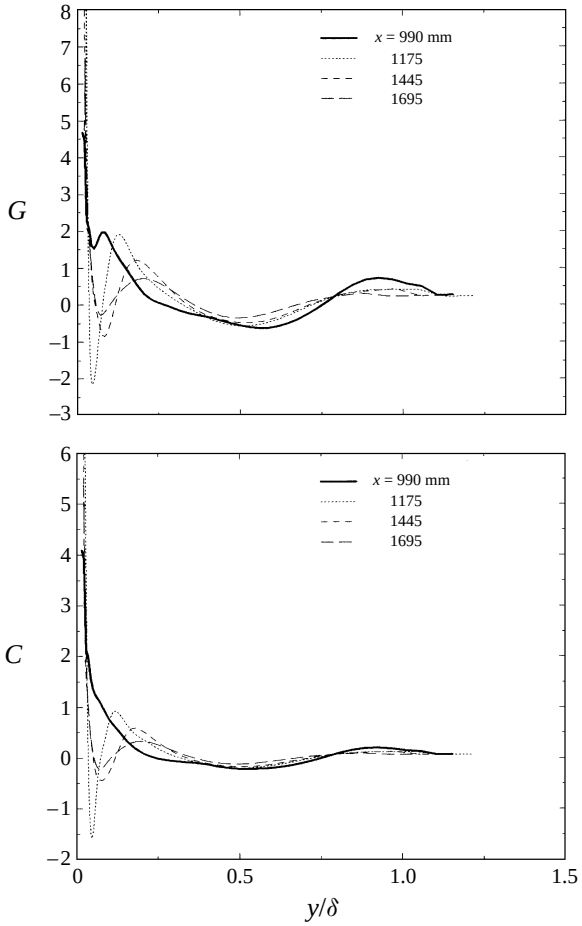

FIGURE 21. Diffusion of turbulent kinetic energy and turbulent transport of shear stress in recovery region.

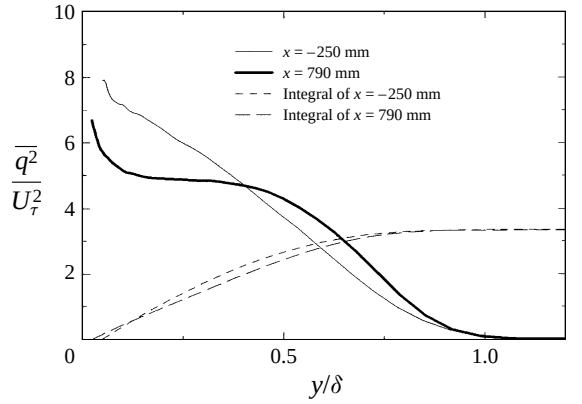

FIGURE 22. Net effect of convergence on the turbulent kinetic energy.

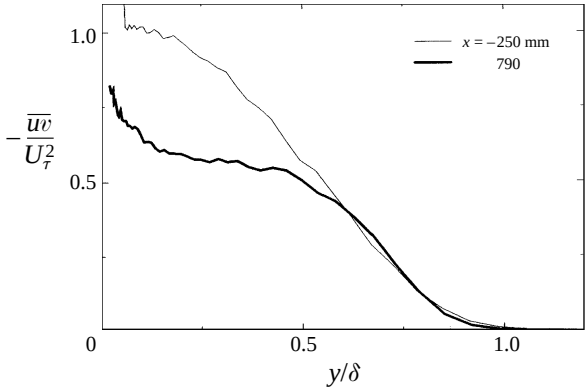

FIGURE 23. Net effect of convergence on the Reynolds shear stress.

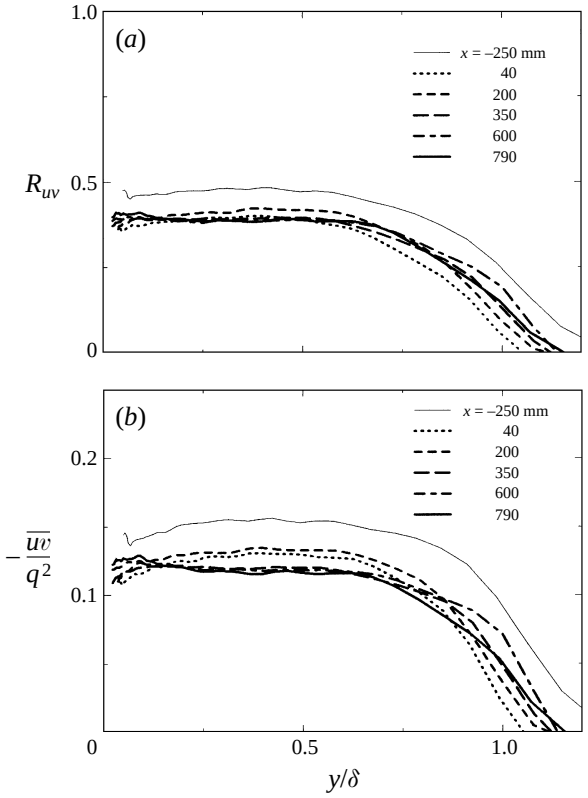

FIGURE 24. Structure parameters in converging section. (*a*) 8 m s^{-1}. (*b*) 20 m s^{-1}.

is possible, however, to make some comments on the behaviour by comparing the behaviour of the other terms. Inspection of the preceding plots suggests that in the inner region the sum of the other measured terms is positive and since the energy is reduced the dissipation (which is negative) must be larger than this sum. In the outer region there is a net gain and hence the dissipation is less than the contributions of the other terms. It may be suggested then that the effect of increasing convergence is to transport energy to the outer flow at a rate which exceeds that of the changes in dissipation and turbulent diffusion. This leads to an imbalance which results in a loss

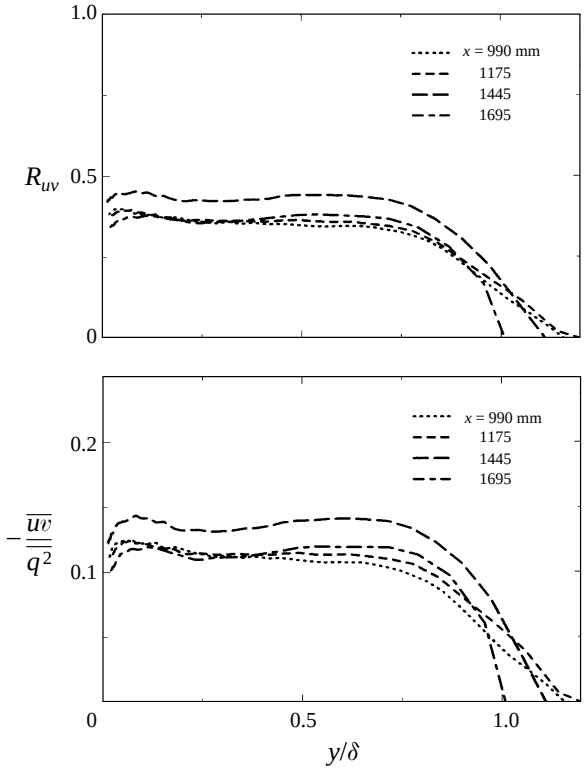

FIGURE 25. Structure parameters in recovery section.

in the inner region and a gain in the outer region. In the Reynolds shear stress there is a definite reduction near the wall but no corresponding increase in the outer flow. This suggests the redistribution due to pressure fluctuation balances the gain due to the extra transport in the outer flow but exceeds the contributions due to the other transport terms in the inner region. By implication the redistribution appears to respond more quickly to the changes in the outer flow than in the inner flow.

6.5. *Recovery*

The results presented show that the recovery of the boundary layer after removal of the convergence is slow. A simple, if crude, estimate of the recovery distance can be made by noting that δ/U_τ is an estimate of the timescale of the boundary layer. Moving in a frame of reference with the free stream gives an estimate of the time 'elapsed' for the flow as x/U_1. Recovery then requires that these two timescales be equal (or at least of something like the same order). This leads to a recovery distance of

$$\left(\frac{x}{\delta}\right)_{\text{recov}} \approx S = U_1/U_\tau. \tag{13}$$

In the present experiment at the end of the converging section $S \approx 28$ for the 8 m s^{-1} case and hence recovery will need a distance of order 28δ which for this case is about 2.8 m. In the 20 m s^{-1} case $S \approx 31$ and so there is little increase (about 10%) in the length required for recovery. This same estimate can also be arrived at by considering the time necessary for the production of kinetic energy equivalent to the kinetic energy of the boundary layer at the end of the converging section.

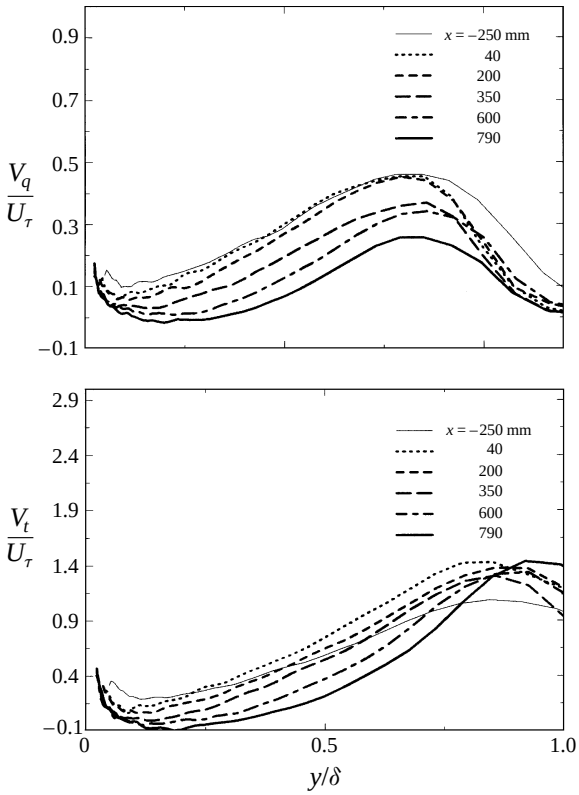

FIGURE 26. Transport velocity of turbulent kinetic energy and Reynolds stress in converging section.

6.6. *The net effect of prolonged convergence*

In order to assess the overall effect of convergence on the turbulent kinetic energy and Reynolds shear stress the first and last measurement stations are examined in this section.

Figure 22 shows the change in kinetic energy of the fluid in the boundary layer between the station in the section before convergence and the last station measured in the converging section. Also shown on this plot are the integrals of the two profiles which show that the total area under the two profiles is the same. The net effect of the prolonged convergence in this experiment has been to redistribute the turbulent kinetic energy from near the wall to the outer flow even when the change in U_τ is taken into account. It should be pointed out that the close coincidence of the two areas also occurs for the 8 m s^{-1} case but does not apply at every station throughout the converging section.

The situation is different for the Reynolds shear stress (figure 23). The net effect appears to be a substantial reduction in the inner region but little, if any, increase in the outer part of the flow. The area under the profile is obviously reduced so the integrals are not plotted for this case.

7. Derived quantities

In this section several parameters of particular relevance to turbulence modelling are presented.

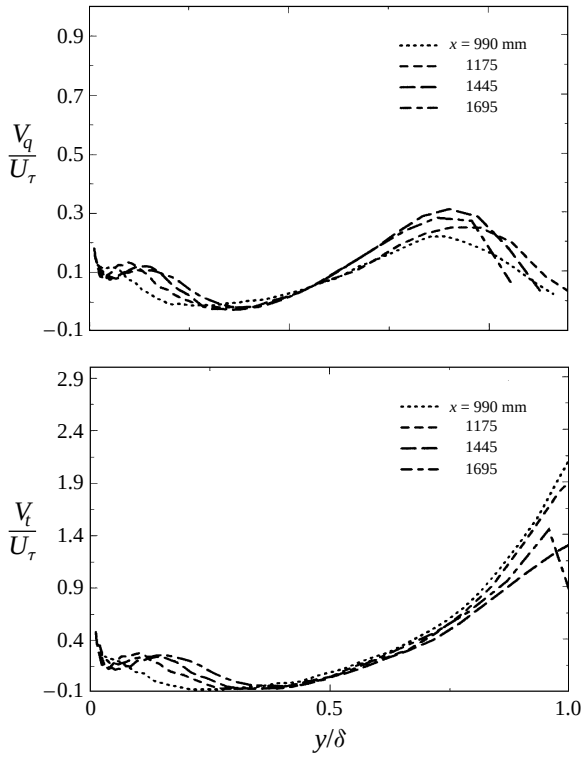

FIGURE 27. Transport velocity of turbulent kinetic energy and Reynolds stress in recovery section.

7.1. *Structure parameters*

The effects of the convergence on the structure of the turbulent boundary layer can be examined by considering the structure parameters. Two important parameters are shown here. The first is $R_{uv} = -\overline{uv}/(\overline{u^2v^2})^{1/2}$ which may be considered to be a measure of the efficiency of turbulent mixing. The second is $-\overline{uv}/\overline{q^2}$ which represents the efficiency of maintenance of the shear stress (Smits *et al.* 1979*a*) and is sometimes used as an empirical input to calculation methods. The results shown in figures 24 and 25 suggest that the effect of convergence on the structure parameters is not large, although there is an initial large decrease in both parameters in the converging region which then appears to settle to a reasonably constant value. In the recovery section the results show, at first, a significant increase, followed by a reduction that leads to profiles which are similar to those at the end of convergence (apart from a small increase in the outer flow).

7.2. *Turbulent transport velocity*

Two other quantities of interest are the transport velocities of turbulent kinetic energy and shear stress. These parameters were suggested by Bradshaw, Ferriss & Atwell (1967) and Bradshaw (1972) as representing the transport of the turbulent kinetic energy and shear stress by convection due to the large eddies of the flow. This definition depends on the large eddies being weak (Bradshaw 1972) and the neglect of the transport by pressure fluctuations. The transport velocities are $V_q = \overline{q^2v}/\overline{q^2}$ for the turbulent kinetic energy and $V_t = \overline{uv^2}/\overline{uv}$ for the Reynolds shear stress. The results given in figures 26 and 27 show a significant reduction of the transport velocity of both kinetic energy and shear stress in the inner region in the converging section which suggests a reduction in the rate at which these quantities are transported away from the

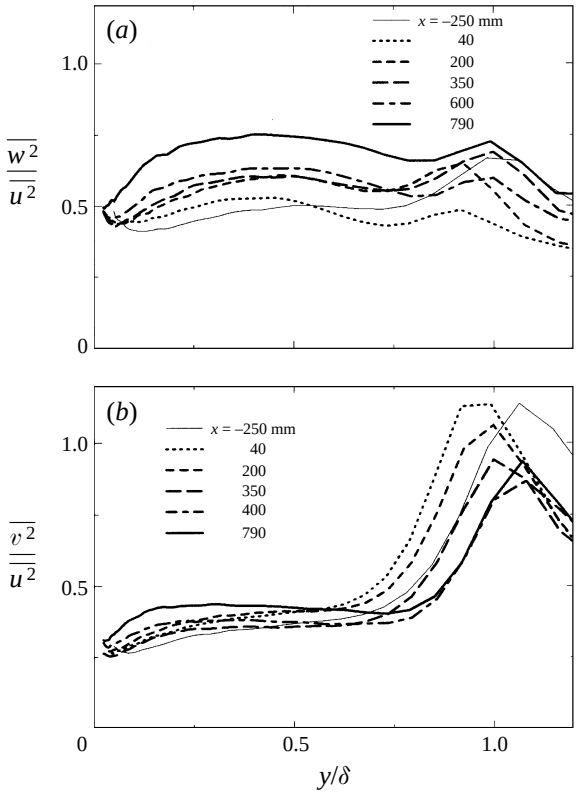

FIGURE 28. Isotropy parameters in converging region. (*a*) 8 m s^{-1}. (*b*) 20 m s^{-1} case.

wall where they are generated. There is also a marked decrease in the outer region in response to the increased advection.

The behaviour in the recovery region reflects the comments made already concerning the full turbulent transport term. There is a distinct increase in the transport velocity near the wall which leads to an increase in the stresses in the inner region where they have been most depleted by the convergence.

7.3. *Reynolds stress ratios*

Figures 28 and 29 show the ratios of the stresses, sometimes called 'isotropy ratios'. In the converging region the results for both Reynolds numbers show an increase in the normal-to-the-wall stress ratio ($\overline{v^2}/\overline{u^2}$) in the inner part of the layer and a decrease in the outer part of the layer. The spanwise stress ratio ($\overline{w^2}/\overline{u^2}$) shows a large overall increase across the layer which is greater in the inner part of the layer. In the recovery region the changes in the Reynolds stress isotropy are much smaller and more difficult to identify within the experimental scatter, although it appears that there is an increase in $\overline{v^2}/\overline{u^2}$ in the outer region of the flow that is opposite to the trend in the converging region.

8. Spectra

The spectra presented here were measured by Saddoughi *et al.* (1991) in the same apparatus and are included for completeness. They illustrate some interesting trends that have not, to the authors' knowledge, been presented before in the open literature.

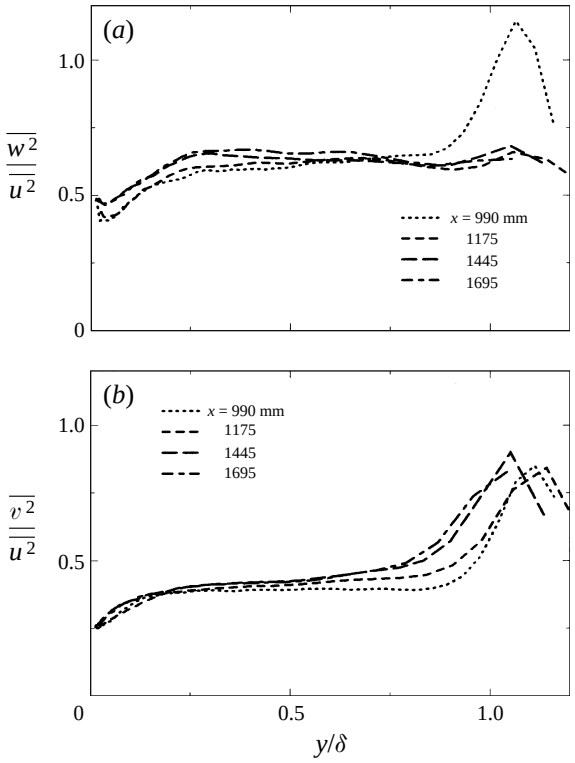

FIGURE 29. Isotropy parameters in recovery region. (*a*) 8 m s^{-1}. (*b*) 20 m s^{-1} case.

Figure 30 shows the spectra for the streamwise component for the upstream parallel flow ($x = -250$ mm) compared with the spectra near the end of the converging section ($x = 790$ mm). The Reynolds numbers at these two stations are significantly different. The plots have been normalized so the area under the graphs is unity and the wavenumber has been calculated from Taylor's hypothesis using a convection velocity equal to the local mean velocity at the point of interest. Throughout the layer there is a significant shift of the energy to higher wavenumbers after convergence which seems to affect all the scales similarly. It has already been noted that the Reynolds number R_θ for these two stations is significantly different. In order to show that this shift is due to convergence the data are compared to the zero pressure-gradient, two-dimensional measurements of Perry & Li (1991) in figure 31. In figure 31(*a*) the spectrum of Perry & Li (1991) at $R_\theta = 11\,100$ and $\eta = 0.058$ is compared with the spectrum at the upstream reference station (zero pressure-gradient, parallel flow) for $R_\theta = 4500$ and $\eta = 0.051$ and it is seen that despite the difference in Reynolds number the spectra are very similar. In figure 31(*b*) the same spectrum of Perry & Li is compared to the station near the end of convergence where the Reynolds number is similar ($R_\theta = 13\,500$ and $\eta = 0.051$). Despite the similar Reynolds number there is still a definite shift toward higher wavenumbers and it would seem that the shift is not due to R_θ effects but is a consequence of convergence. It is interesting to note that Saddoughi & Joubert (1991) observed a shift of energy toward lower wavenumbers for the diverging flow which is opposite to the trend observed here. The reason for this shift is not yet known. It should be noted that, since the streamwise wavenumber was calculated using Taylor's hypothesis, a shift of the spectra could simply indicate a change in the convection

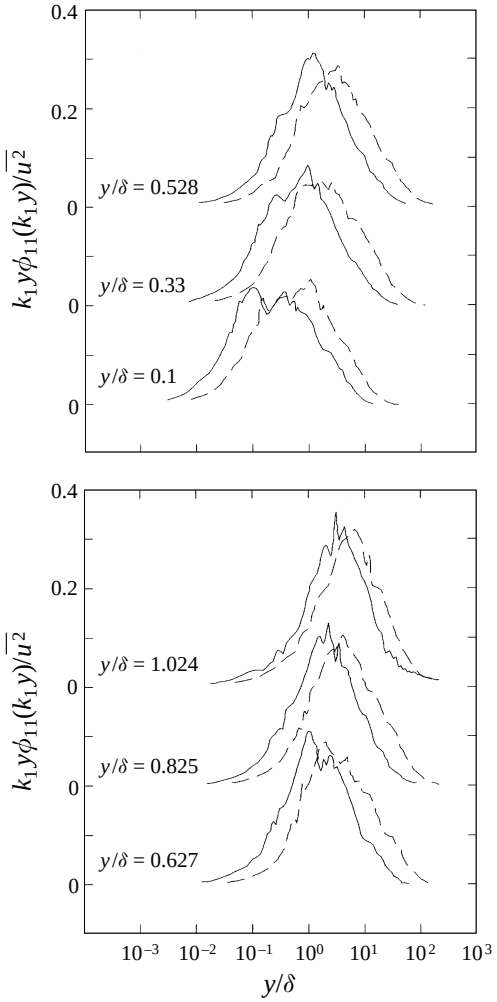

FIGURE 30. Premultiplied spectra. ——, upstream station before convergence; – – –, $x = 790$ mm after prolonged convergence.

velocity from the value assumed which is the local mean velocity at the point of interest.

9. Conclusions

The effects of lateral streamline convergence on boundary layers developing in a zero pressure gradient have been presented. It has been shown that the local effect of convergence (or divergence) can be characterized in terms of a single equilibrium parameter β_D. In the results presented this parameter increases rapidly with streamwise distance which leads to large changes in the mean flow and turbulence quantities whereas in the results of Saddoughi *et al.* 1991) for diverging flow of the same included angle the parameter becomes approximately constant and the flow reaches a state of apparent equilibrium. This supports the contention that β_D is an equilibrium parameter. The effects of positive β_D in this experiment shows some similarities to the

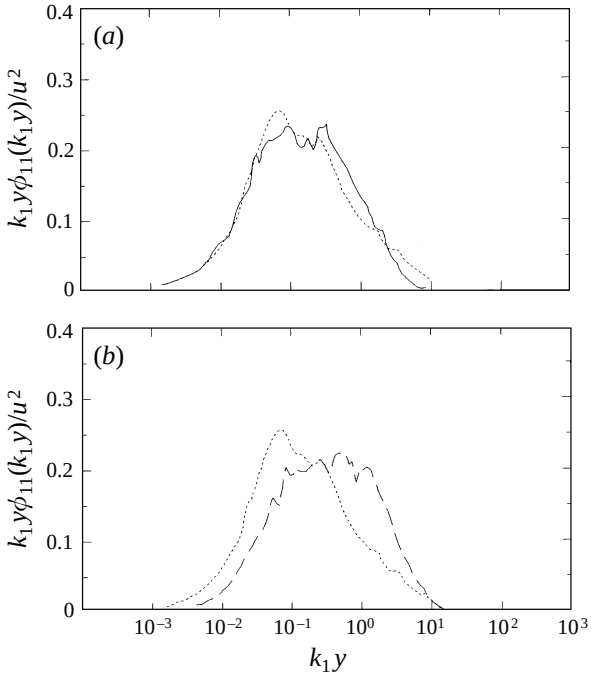

FIGURE 31. Premultiplied spectra. (*a*) · · ·, data of Perry & Li (1991) $R_\theta = 11\,100$, $y/\delta = 0.058$, ——, upstream station present case $R_\theta = 4500$, $y/\delta = 0.051$. (*b*) · · ·, data of Perry & Li (1991) $R_\theta = 11\,100$, $y/\delta = 0.058$, – – –, $x = 790$ mm present case $R_\theta = 13\,500$, $y/\delta = 0.051$.

effects of positive β_x in two-dimensional boundary layers (i.e. adverse pressure gradient flows). This is probably due to the fact that they affect $\partial V/\partial y$ similarly.

In this experiment the increase of β_D leads to a significant reduction of the skin friction compared with a zero pressure-gradient layer without convergence and an increase in the boundary-layer thickness. This is accompanied by an increase in the Coles wake factor (Π).

The results also show a significant reduction of the Reynolds stresses in the inner region of the flow ($0.1 < \eta < 0.4$) and an increase in the turbulent kinetic energy in the outer part of the flow. It is shown that the principal effects leading to these changes are an 'immediate' reduction in both the generation of shear stress and the production of kinetic energy and an increase in advection by the mean flow. The changes in turbulent transport are opposite to those of the advection and appear to be a response of the boundary layer in order to compensate for the changes in the other transport terms (i.e. an attempt to restore equilibrium). In the present experiment β_D is increasing rapidly and the changes in turbulent transport are not sufficient to redistribute the energy and shear stress which leads to significant changes in the shape of the Reynolds stress profiles.

Recovery after convergence is shown to be characterized by an increased transport from the region very close to the wall to the region where the stresses have been depleted. This recovery is slow since it depends on the time-scale of the large eddies. An important conclusion of this work is that changes in turbulence structure of a boundary layer, due to convergence or divergence, depends strongly on the rate-of-change of the equilibrium parameter, β_D and the timescale of the large eddies in the flow. It should also be noted that the concept of convergence as a 'stabilizing' influence

must be revised since the stresses are redistributed rather than simply suppressed. In the outer region of the flow where the Bradshaw parameter, B, is large the stresses actually increase and they decrease near the wall where this parameter is small. This reflects the fact that B is a local parameter and significant changes occur owing to non-local effects such as advection and turbulent transport.

Spectral measurements show an apparent shift in energy to higher wavenumbers although, at this stage, the reason for this shift is not known.

This project was financially supported by the Australian Research Council. The authors' would also like to thank Dr S. Hafez and Dr S. G. Saddoughi since the present work benefited from their preliminary study.

REFERENCES

Bradshaw, P. 1967 The turbulence structure of equilibrium boundary layers. *J. Fluid Mech.* **29**, 625–645.

Bradshaw, P. 1972 The understanding and prediction of turbulent flow. *Aero. J.* **76**, 403–418.

Bradshaw, P. 1973 Effects of streamline curvature on turbulent flow. *AGARDograph* **196**, 1–80.

Bradshaw, P., Ferriss, D. H. & Atwell, N. P. 1967 Calculation of boundary-layer development using the turbulent energy equation. *J. Fluid Mech.* **28**, 593–616.

Clauser, F. H. 1954 Turbulent boundary layers in adverse pressure gradients. *J. Aero. Sci.* **21**, 91–108.

Clauser, F. H. 1956 The turbulent boundary layer. *Adv. Appl. Mech.* **4**, 1–51.

Das, D. K. 1987 A numerical study of turbulent separated flows. *Am. Soc. Mech. Engng forum on turbulent flows*, FED **51**, 85–90.

East, L. F., Sawyer, W. G. & Nash, C. R. 1979 An investigation of the structure of equilibrium turbulent boundary layers. *RAE Tech. Rep.* 79040.

Erm, L. P. & Joubert, P. N. 1991 Low-Reynolds-number turbulent boundary layers. *J. Fluid Mech.* **230**, 1–44.

Kármán, T. von 1932 *Theorie des Reibungswiderstands*, *Hydromechanische Probleme des Schiffsantriebs*. pp. 50–73. Hamburg.

Hafez, S. & Joubert, P. N. 1992 Some aspects of the effects of streamline convergence on a fully developed turbulent boundary layer. *11th Australasian Fluid Mech. Conf.*, *University of Tasmania*, *Hobart*, *Australia*, pp. 551–554.

Lawn, C. J. 1971 The determination of the rate of dissipation in turbulent pipe flow. *J. Fluid Mech.* **48**, 477–505.

Nickels, T. B. & Joubert, P. N. 1997 Equilibrium layers with extra rates-of-strain. Submitted to *J. Fluid Mech.*

Perry, A. E. 1982 *Hot Wire Anemometry*. Oxford University Press.

Perry, A. E. & Li, J. D. 1991 Experimental support for the attached-eddy hypothesis in zero-pressure-gradient turbulent boundary layers. *J. Fluid Mech.* **218**, 405–438.

Pompeo, L., Bettelini, M. S. G. & Thomann, H. 1993 Laterally strained turbulent boundary layers near a plane of symmetry. *J. Fluid Mech.* **257**, 507–532.

Rotta, J. C. 1962 Turbulent boundary layers in incompressible flow. *Prog. Aero. Sci.* **2**, 1–212.

Saddoughi, S. G. & Joubert, P. N. 1991 Lateral straining of turbulent boundary layers. Part 1. Streamline divergence. *J. Fluid Mech.* **229**, 173–204.

Saddoughi, S. G. 1988 Experimental studies of the effects of streamline divergence on developing turbulent boundary layers. PhD thesis, Mech. Engng, The University of Melbourne.

Saddoughi, S. G., Hafez, S. & Joubert, P. N. 1991 Some preliminary results for the effects of streamline convergence on a fully developed turbulent boundary layer. *2nd Osaka Int. Coll. Visc. Fluid Dyn. and Ship Ocean Tech.*

Sjolander, S. A. 1980 Eddy viscosity in two-dimensional and laterally strained boundary layers. PhD dissertation, University of Cambridge.

SMITS, A. J., EATON, J. A. & BRADSHAW, P. 1979*a* The response of a turbulent boundary layer to lateral divergence. *J. Fluid Mech.* **94**, 243–268.

SMITS, A. J., YOUNG, S. T. & BRADSHAW, P. 1979*b* The effect of short regions of high surface curvature on turbulent boundary layers. *J. Fluid Mech.* **94**, 209–242.